

Original Research

Numerical-Analytical Method for Predicting Water Inflow into the Tunnel through Conductive Fault Fracture Zone

Jianhua Wang¹, Hongliang Liu², Wenfeng Tu^{2*}, Cong Mou¹, Xing Wan¹

¹School of Transportation, Southeast University, Nanjing, China

²School of Qilu Transportation, Shandong University, Jinan, China

Received: 22 December 2022

Accepted: 18 February 2023

Abstract

Water inrush is commonly encountered while tunnelling through a conductive fault fracture zone, and seriously affects the hydrogeological environment around the tunnel. This paper proposed a new method to predict water inflow during the water inrush. Firstly, a unified time-dependent constitutive model considering Darcy flow and non-Darcy flow in the fault fracture zone was established, and the numerical time-variant water inflow was analyzed. Secondly, the analytical prediction of time-variant water inflow was conducted, which was compared with the numerical results and the measured data. The numerical and analytical prediction method was found to be reliable for the water inflow into the tunnel through the conductive fault fracture zone. On this basis, a combined numerical-analytical method for predicting water inflow was proposed and a reasonable prediction range of water inflow was constructed. Furthermore, the modified time-variant water inflow prediction method was developed by incorporating the temporal and spatial variation in the hydraulic conductivity. The modified prediction range of water inflow can be more consistent with the measured water inflow. The results show that the prediction accuracy of water inflow can be improved by considering the depth effect of hydraulic conductivity in the fault fracture zone for this typical case.

Keywords: water inflow, fault fracture zone, numerical and analytical prediction, temporal and spatial variation in the hydraulic conductivity, modified prediction

Introduction

The geological disaster known as water inrush is commonly encountered while tunnelling through a conductive fault fracture zone, and seriously affects the hydrogeological environment around the tunnel [1, 2].

A reliable prediction of groundwater inflow into a tunnel is a core issue for the design and construction of tunnel excavation [3, 4]. On one hand, the drainage facilities, lining form and reinforcement range of grouting need to be designed regarding the predicted water inflow in the design stage [5-7]. On the other, the construction progress and water-blocking measures need to be adjusted based on the predicted water inflow in the construction stage [8]. Therefore, the study

*e-mail: wenfengtu@sdu.edu.cn

of water inflow prediction is of great practical significance for safe construction in tunnel engineering.

When the tunnel passes through the conductive fault fracture zone, the groundwater level of the fault fracture zone is subjected to an excavation-induced drawdown [1, 9, 10]. Generally, the water table of the fault fracture zone must be drawn down gradually to the level of the heading from the initial groundwater level. The level of the drawdown cone and water inflow will get lower and smaller, and finally reach a steady state as time increases [1]. Therefore, the prediction method of water flow into tunnel needs to account for the time-variant flow.

Empirical, analytical and numerical methods are usually adopted to predict the water inflow into the tunnel [11-15]. The amount of water inflow is predicted in the whole tunnel based on some simplifying assumptions, and the average unit water inflow can be obtained. However, most of the methods do not adequately account for the effect of regional geotechnical conditions near the fault fracture zone. Moreover, the previous studies are limited to predict the water inflow at a specific point in time (e.g., maximum water inflow and steady-state water inflow), and it is impossible to accurately judge the water inflow time history before the water inflow reaches the steady state. The prediction of the time-variant water inflow is essential under the geological conditions of the conductive fault fracture zone, which can promote the timely treatment of water inrush disasters.

Numerical methods like the finite element method (FEM), finite difference method (FDM), and discrete element method (DEM) have been widely used to model complex geotechnical conditions [16-18]. For the water inrush induced by the conductive fault fracture zone, hydraulic conductivity is one of the fundamental properties, which governs the seepage behavior during the water inrush [1, 19]. It remains to be verified whether Darcy's law describes water flow in the fault fracture zone accurately. In addition, the variation of hydraulic conductivity with space and time needs to be considered in the fault fracture zone in the prediction. The space-dependent hydraulic conductivity reflects the stress-induced rock-mass permeability reduction along the depth of the fault fracture zone [20], and the time-dependent hydraulic conductivity reflects the increased porosity caused by particle loss during water inrush [21]. Furthermore, its corresponding temporal and spatial variation of hydraulic conductivity on the water inflow needs to be studied in the water inflow prediction when designing the grouting of tunnels.

This paper proposes a time-dependent unified constitutive equation for the water flow, and the numerical water inflow prediction model when the tunnel passes through the conductive fault fracture zone is developed for both transient and steady-state regimes. The dynamic variation law of water inflow into the tunnel is analyzed. Combined with the analytical water inflow prediction, a comprehensive prediction method

of water inflow is proposed. Furthermore, given the temporal and spatial variation of hydraulic conductivity in the fault fracture zone, a modified method of water inflow prediction which can improve the prediction accuracy of water inflow is proposed.

Methods

Numerical Water Inflow Prediction

Numerical Modelling

The numerical model is developed based on a typical case of a tunnel, which passes through the fault fracture zone [1], as shown in Fig. 1. The fault fracture zone width (B) is 15 m, the dip angle (θ) is 78° , the hydraulic conductivity of recharge aquifer (K_1) is 1×10^{-5} m/s, and the water storage coefficient ratio of recharge aquifer (S_{S1}) is 1×10^{-4} . By contrast, the hydraulic conductivity of the fault fracture zone (K) is 1.2×10^{-4} m/s and the storage coefficient ratio of the fault fractured zone (S_S) is 1×10^{-4} . The radius of the tunnel is 5.9 m. The initial hydraulic heads of the recharge aquifer and the fault fracture zone are both 375 m ($t = 0$, $H_1 = H = 375$ m), and the drawdown at the tunnel heading (D) is 250 m. In the numerical model, the equivalent continuum media model is adopted, groundwater flow patterns in the recharge aquifer and fault fracture zone are respectively defined as Darcy flow and non-Darcy flow, respectively.

The left, right and lower boundaries are considered as the impermeable boundaries, $nK\nabla H = 0$, $nK_1\nabla H_1 = 0$; the upper boundary is considered as the constant hydraulic head boundary, $H = H_1 = 375$ m; the contact surfaces of the fault fracture zone are treated as the continuous boundaries, $nK_1\nabla H_1 = -nK\nabla H$ and $H_1 = H$; the tunnel heading is the permeable boundary

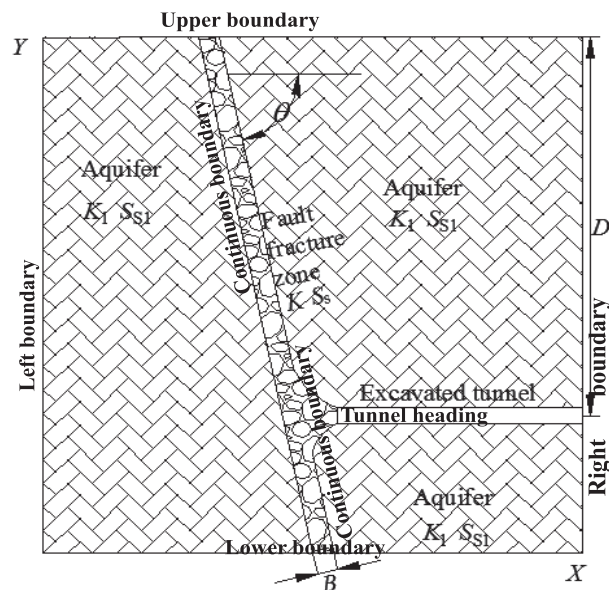


Fig. 1. The numerical model of the water inflow prediction.

$H = Y_{\text{tunnel}}$, where Y_{tunnel} is the elevation head of the excavated tunnel).

Numerical Constitutive Equation

Choosing a reasonable governing equation to describe the water flow in the fault fracture zone is crucial for the numerical prediction of water inflow. To obtain the governing equation, the following assumptions are made: (1) Fault fracture zone is considered as an equivalent continuous medium, groundwater in fault fracture zone is equally distributed; (2) Hydraulic conductivity is only related to the porosity and fluid properties for Darcy flow, while that is not constant and is related to the hydraulic gradient for non-Darcy flow.

Forchheimer quadratic relationship between the hydraulic gradient and the seepage velocity is more reasonable for non-Darcy flow in the fault fracture zone [22-24], for which expression is shown in Eq. (1). At low-flow velocity, the first term (Darcy flow term) plays a leading role, where the flow is linear. At high-velocity flow, however, the second term dominates and becomes non-linear.

$$J = \frac{\mu}{\rho g k} v + \frac{\beta}{g} v^2 \tag{1}$$

where J is the hydraulic gradient; μ is the dynamic viscosity; k is the permeability, $k = \mu K / \rho g$; g is the gravity coefficient; v is the flow velocity; β is the non-Darcy flow influencing coefficient.

In order to put forward the unified form of Darcy flow and non-Darcy flow, hydraulic conductivity is assumed as a variable parameter which is related to the hydraulic gradient in the non-Darcy flow. Darcy flow and non-Darcy flow are expressed as a unified form of $v = K(J) J$, Eq. (1) can be transformed into

$$v = \left\{ -\frac{\mu}{2k\rho\beta} + \left[\left(\frac{\mu}{2k\rho\beta} \right)^2 + \frac{g}{\beta} J \right]^{\frac{1}{2}} \right\} J^{-1} * J \tag{2}$$

Wang et al. proposed that the relationship between k and β could be determined by the smooth parallel plate tests [23], which was described as

$$\beta = 0.0003k^{-0.6134} \tag{3}$$

According to the equivalent continuum seepage principle, the governing equation of Darcy flow is shown in Eq. (4).

$$\frac{\partial(K \frac{\partial H}{\partial x})}{\partial x} + \frac{\partial(K \frac{\partial H}{\partial y})}{\partial y} = S_s \frac{\partial H}{\partial t} \tag{4}$$

where H represents the hydraulic head of fault fracture zone and is equal to the sum of the pressure head and elevation head; K is the hydraulic conductivity; S_s is the storage coefficient ratio of aquifer.

According to Eqs. (3) and (4), the unified governing equation of Darcy and non-Darcy flow in the fault fracture zone can be deduced as follows:

$$\frac{\partial(K(J) \frac{\partial H}{\partial x})}{\partial x} + \frac{\partial(K(J) \frac{\partial H}{\partial y})}{\partial y} = S_s \frac{\partial H}{\partial t} \tag{5}$$

$$K(J) = J^{-1} \left\{ -\frac{\mu}{2k\rho\beta} + \left[\left(\frac{\mu}{2k\rho\beta} \right)^2 + \frac{g}{\beta} J \right]^{\frac{1}{2}} \right\} \tag{6}$$

Numerical Prediction Results

In case of non-Darcy component of flow, hydraulic conductivity is not constant, but changes significantly with the hydraulic gradient. Eq. (5) is highly non-linear without the general solution for the corresponding boundary conditions and initial conditions. Therefore, the finite-element (FE) solver in the PDE module of COMSOL Multiphysics, a commercial FE software, was used to predict the water inflow into the tunnel.

Fig. 2 shows the distribution of hydraulic head during the process when groundwater flows into the tunnel from the fault fracture zone in the Darcy flow and non-Darcy flow, respectively. The hydraulic head of the fault fracture zone and recharge aquifer decreases gradually with the continuous water inflow into the tunnel, and the drawdown cone gradually develops to a steady state. As noticed, the development of the drawdown cone in the non-Darcy flow pattern is significantly faster than that in the Darcy flow pattern, which conforms to the high-velocity flow characteristics. It is demonstrated that the unified constitutive model can well describe the flow of groundwater in the fault fracture zone under different flow conditions.

Fig. 3 presents the mean flow velocity and water inflow during the water inrush induced by the conductive fault fracture zone. The flow velocity sets are formed by extracting the flow velocity at each position of the heading surface in the tunnel excavation, as shown in Fig. 3 a) and c). Thus, the instantaneous mean flow velocities of the heading surface in the Darcy flow and non-Darcy flow patterns are also obtained, respectively. Obviously, the mean water inflow in the Darcy flow pattern is obviously less than that in the non-Darcy pattern, as shown in Fig. 3 b) and d).

Analytical Water Inflow Prediction

Analytical Prediction Method

Hwang and Lu proposed the semi-analytical method for the prediction of the water inflow method [1].

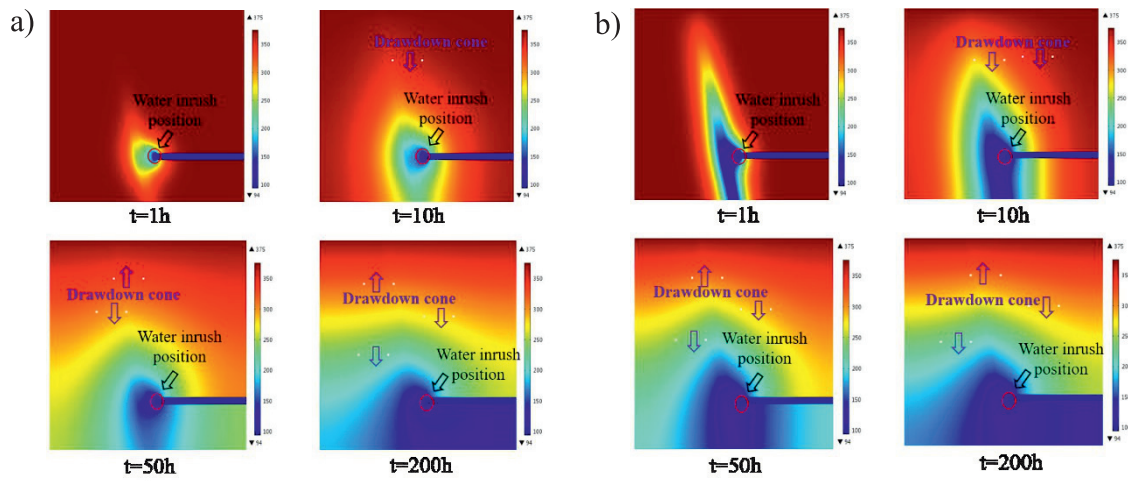


Fig. 2. Cloud charts of hydraulic head evolution: a) Darcy flow in the fault fracture zone, b) Non-Darcy flow in the fault fracture zone.

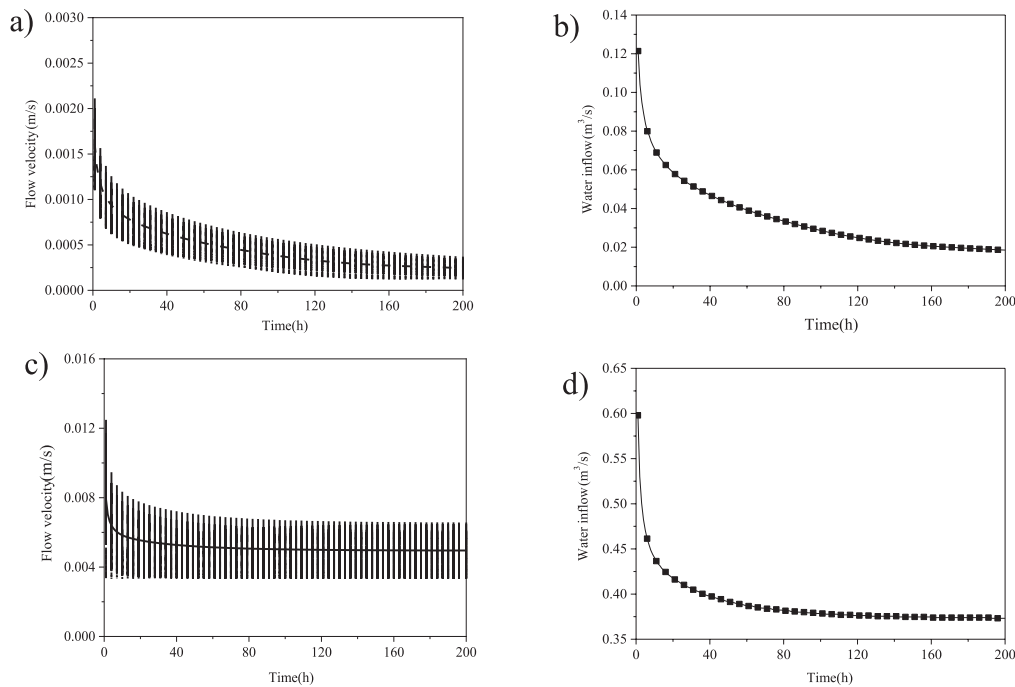


Fig. 3. Numerical prediction curves of mean flow velocity and water inflow: a) Mean flow velocity of Darcy flow, b) Mean water inflow of Darcy flow, c) Mean flow velocity of non-Darcy flow, d) Mean water inflow of non-Darcy flow.

The induced water inflow when the tunnel passes through the fault fracture zone can be calculated by the image method and the superposition principle. Using these methods, the tunnel inflow problem in a finite flow domain can be transformed to the problem in the infinite flow domain. The analytical method is shown in Eq. (7). Note that groundwater recharge from the surrounding aquifer to the fault fracture zone is not considered.

$$Q(t_i) = Q(t_{i-1}) + \frac{D - \sum_{j=1}^{i-1} [Q(t_j) - Q(t_{j-1})] F(P, r_0, t_i - t_{j-1})}{F(P, r_0, t_i - t_{i-1})} \quad (7)$$

$$F(P, r_0, t_i - t_j) = \frac{1}{2\pi K} \sum_{n=-\infty}^{\infty} (erfc(u_n) / r_n) + \frac{1}{2\pi K} \sum_{n=-\infty}^{\infty} (erfc(u'_n) / r'_n) \quad (8)$$

$$erfc(u) = \frac{2}{\sqrt{\pi}} \int_u^{\infty} e^{-x^2} dx \quad (9)$$

where $Q(t_0) = 0$; $Q(t_1) = D/F(P, r_0, t_1)$; $u_n = r_n / (4\lambda\Delta t_{ij})^{1/2}$; $r_n = 2nB$; if $n = 0$, $r_n = r_0$; $u'_n = r'_n / (4\lambda\Delta t_{ij})^{1/2}$; $r'_n = ((2nB\cos\theta + 2D)^2 + (2nB\sin\theta)^2)^{1/2}$; $\lambda = K/S_s$. B is the thickness of the fault fracture zone; λ is the hydraulic diffusivity of the fault fracture

zone; S_s is the specific storage coefficient; $erfc$ is the complementary error function as shown in Eq. (9).

The accuracy of the solution of Eq. (7) depends on the number of the series term n used in the calculation. In order to satisfy the required accuracy, the number of series terms n needs to reach 20 and the calculated result needs to converge in this case. The predicted time series of the water inflow are shown in Fig. 4, it can be observed that the predicted water inflow decreases significantly during the first 50 hours, which then moderates gradually with a stable value of about $0.56 \text{ m}^3/\text{s}$.

Comparison between Analytical and Numerical Predictions

The reliability of the analytical method has been verified for predicting water inflow [1]. The predicted water inflow by the combined numerical-analytical

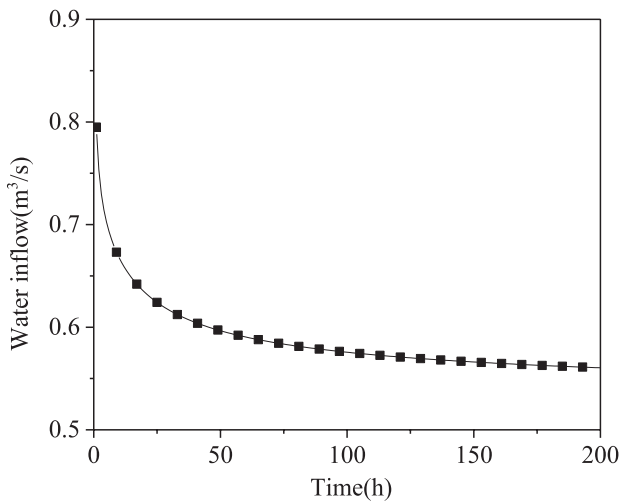


Fig. 4. Analytical prediction curves of water inflow.

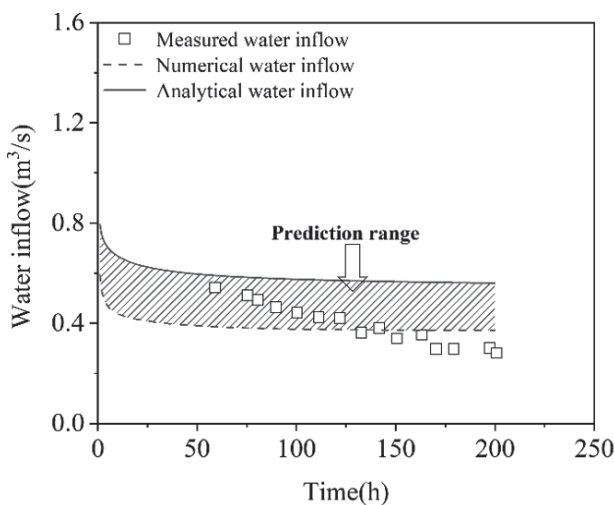


Fig. 5. Combined numerical-analytical prediction of the water inflow.

method is compared with the measured inflow, as shown in Fig. 5. The comparisons among the analytical, numerical, and measured water inflow demonstrate that the predicted water inflow captures the general trend of the measured water inflow. Meanwhile, the rationality of the proposed unified groundwater constitutive equation in the numerical water inflow prediction can be verified. Therefore, it is considered that the proposed numerical-analytical method provides a reliable tool for the water inflow prediction when the tunnel passes through the conductive fault fracture zone. Note that the prediction errors between the numerical and analytical methods for water inflow are caused by different basic assumptions.

Results and Discussion

Modified Water Inflow Considering Time Effect on Hydraulic Conductivity

It is accepted that hydraulic conductivity is the key parameter for the prediction of water inflow [1, 20]. Notably, the time-dependent hydraulic conductivity reflects that the solid particles in the fault fracture zone will migrate and lose with the water flow during the water inrush, which can result in an increase in the porosity of the fault fracture zone. The hydraulic conductivity of the fault fracture zone gradually increases to the ultimate value over time. Thus, the time effect on hydraulic conductivity should be considered in the prediction. The schematic illustration of the analytical solution is shown in Fig. 6. The quantitative relationship of the hydraulic conductivity varying with time is shown in Eq. (10) [25].

$$K = \begin{cases} K_0 \exp(\alpha t) & t < t_f \\ K_{\max} & t > t_f \end{cases} \quad (10)$$

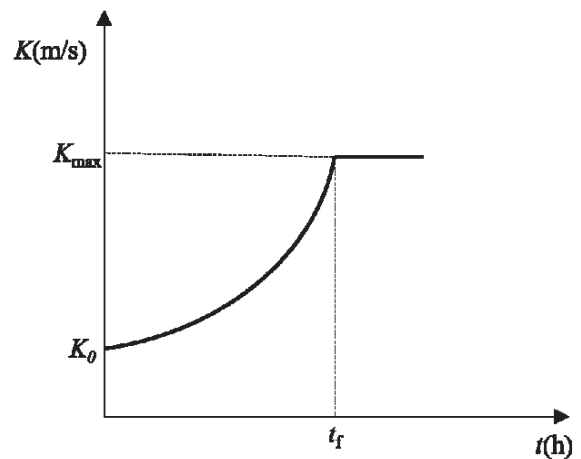


Fig. 6. Schematic diagram of the time-dependent hydraulic conductivity.

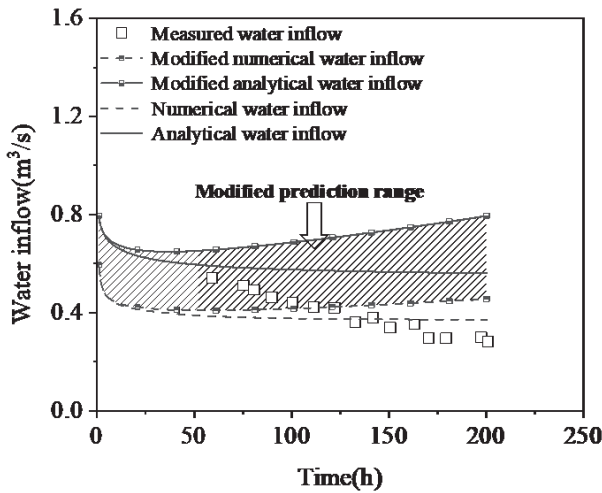


Fig. 7. Modified prediction of the water inflow with time-related factor $\alpha = 0.04 \text{ d}^{-1}$.

where K_0 is the initial hydraulic conductivity of fault fracture zone; K_{\max} is the maximum hydraulic conductivity of fault fracture zone; α is the time-related factor. The seepage erosion effect on the permeability becomes more predominant with the increasing time-related factor α . t_f is the time for the fully-developed water inrush channel in the fault fracture zone. When $t < t_f$ the process is that the hydraulic conductivity of water inrush channel increases gradually; when $t \geq t_f$ the hydraulic conductivity is constant.

As shown in Fig. 7, the modified prediction of the time-variant water inflow considering the time effect on hydraulic conductivity is generally greater than the above combined numerical-analytical prediction. In addition, the modified water inflow prediction range is close to the combined prediction range with a smaller time-related factor (e.g., $\alpha = 0.04 \text{ d}^{-1}$). Thus, the prediction accuracy of water inflow considering the time effect on hydraulic conductivity can no further be improved compared with the measured ones. In other words, there is no obvious loss of solid particles in the fracture zone for this solution.

Modified Water Inflow Considering Depth Effect on Hydraulic Conductivity

Moreover, the space-dependent hydraulic conductivity model exhibits different hydraulic conductivity at different depths in the fault fracture zone based on the site investigation [26-28], as shown in Fig. 8. The hydraulic conductivity of fault fracture zone is mainly affected by stress level and weathering degree. Specifically, the fracture aperture of fault fracture zone changes due to the different stress levels in different buried depths. Higher stress level leads to more closed cracks, thus inducing lower hydraulic conductivity. In addition, the rock mass deeply buried in the fault fracture zone has a low degree of weathering and

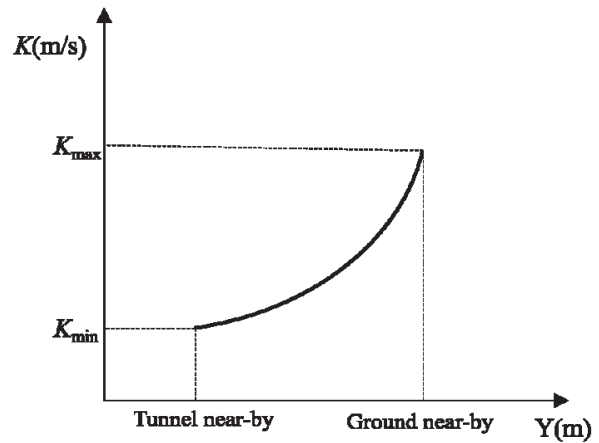


Fig. 8. Schematic diagram of the space-dependent hydraulic conductivity.

thus exhibits lower hydraulic conductivity. However, the rock mass near the ground surface develops more cracks due to weathering, resulting in higher hydraulic conductivity. Hydraulic conductivity decreases along with the depth of the fault fracture zone, sometimes accompanies with a difference of several orders of magnitude. The exponential model is the most widely-used empirical formula, which can be expressed as follows:

$$K_x(x, y) = K_y(x, y) = K_{\text{ground}} [-A(y_s(x) - y)] \quad (11)$$

where $K_x(x, y)$ and $K_y(x, y)$ are the components of the hydraulic conductivity K tensor; K_{ground} is the hydraulic conductivity at the ground surface; A is the depth-related factor; $y_s(x)$ is a function of the ground surface elevation.

As shown in Fig. 9, the modified prediction of time-variant water inflow is less than the combined

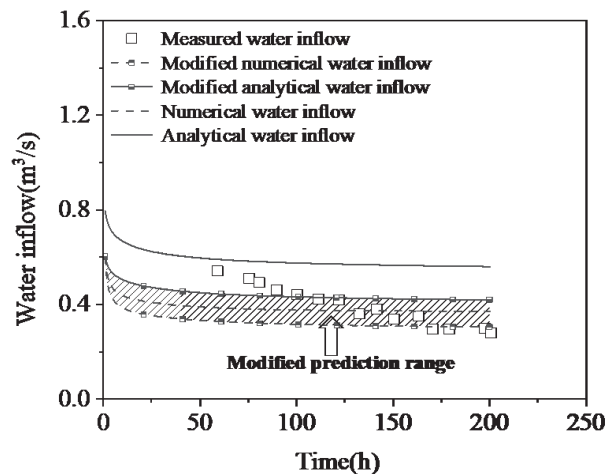


Fig. 9. Modified prediction of the water inflow with depth-related factor $A = 0.0012 \text{ m}^{-1}$.

prediction when the depth effect of hydraulic conductivity is considered in the prediction. Meanwhile, the range of the time-variant water inflow predicted by the modified numerical-analytical method is closer to the measured water inflow with a depth-related factor (A) of 0.0012 m^{-1} . A more reasonable prediction range is determined. In other words, the modified prediction method considering the depth effect on the hydraulic conductivity in the fault fracture zone can further improve the accuracy of water inflow prediction compared with the measured ones for this simulation. It should be noted that there is a large error between the predicted water inflow and the measured water inflow at the initial stage of water inrush, which needs to be further optimized in future research.

Conclusions

For the water inrush when the excavated tunnel passes through the conductive fault fracture zone, the study on the water inflow prediction is the key issue to guide the water inrush prevention. This paper presented a combined analytical-numerical method for the calculation of water inflow into the tunnel through the conductive fault fracture zone. The conclusions are as follows:

(1) In this paper, a unified constitutive model of Darcy and non-Darcy flow is established, and the time-variant water inflow is numerically predicted. Meanwhile, the analytical time-variant water inflow is also calculated using image method and superposition principle. Thus, a combined numerical-analytical method for predicting water inflow was proposed by comparison with the measured water inflow. A reasonable prediction range of water inflow was constructed

(2) The modified method of water inflow prediction is discussed. The temporal and spatial variation in the hydraulic conductivity is considered based on the combined numerical-analytical water inflow prediction. The results show that the prediction accuracy of water inflow can be further improved by considering the depth effect on the hydraulic conductivity in the conductive fault fracture zone for this typical practice. A more reasonable prediction range is optimized to meet the long-lasting water inflow except for the initial stage.

Acknowledgements

This work was supported by the International Postdoctoral Exchange Fellowship Program from China Postdoctoral Council (PC2021016). The authors would like to express appreciation to the reviewers for their valuable comments and suggestions that helped improve the quality of the paper.

Conflict of Interest

The authors declare no conflict of interest

Notes

A	depth-related factor of hydraulic conductivity
B	thickness of fault fracture zone
g	gravity coefficient
H	hydraulic head of fault fracture zone
K	hydraulic conductivity of fault fracture zone
K_0	initial hydraulic conductivity of fault fracture zone
K_{ground}	hydraulic conductivity at ground surface
K_{max}	maximum hydraulic conductivity of fault fracture zone
$K_x(x, y)$	component of the hydraulic conductivity K tensor in x direction
$K_y(x, y)$	component of the hydraulic conductivity K tensor in y direction
J	hydraulic gradient
S_s	storage coefficient ratio of fault fracture zone
S_{s1}	storage coefficient ratio of recharge aquifer
t_f	time for fully-developed water inrush channel in fault fracture zone
α	time-related factor of hydraulic conductivity
β	non-Darcy flow influencing coefficient
λ	hydraulic diffusivity of fault fracture zone

References

- HWANG J.H., LU C.C. A semi-analytical method for analyzing the tunnel water inflow. *Tunnel and Underground Space Technology*, **22** (1), 39, **2007**.
- LI S.C., GAO C.L., ZHOU Z.Q., LI L.P., WANG M.X., YUAN Y.C., WANG J. Analysis on the precursor information of water inrush in karst tunnels: A true triaxial model test study. *Rock Mechanics and Rock Engineering*, **52** (2), 373, **2019**.
- LI D.Y., LI X.B., LI C.C., HUANG B.R., GONG F.Q., ZHANG W. Case studies of groundwater flow into tunnels and an innovative water-gathering system for water drainage. *Tunnel and Underground Space Technology*, **24** (3), 260, **2009**.
- GOLIAN M., KATIBEH H., SINGH V.P., OSTAD-ALI-ASKARI K., ROSTAMI H.T. Prediction of tunnelling impact on flow rates of adjacent extraction water wells. *Quarterly Journal of Engineering Geology and Hydrogeology*, **53** (2), 236, **2020**.
- ZHANG Q.S., HAN W.W., LI S.C., YUAN Y.R., LIU R.T., LI J.Q., SUN H.F. Comprehensive grouting treatment for water gushing analysis in limestone breccias fracture zone.

- Chinese Journal of Rock Mechanics and Engineering, **31** (12), 2412, **2012**.
6. ZHANG Q.S., ZHANG L.Z., LIU R.T., HAN W.W., Zhu M.T., LI X.H., ZHNEG D.Z., Xu X.H. Laboratory experimental study of cement-silicate slurry diffusion law of crack grouting with dynamic water. *Rock and Soil Mechanics*, **36** (8), 2159, **2015**.
 7. LI P., ZHANG Q.S., SUN L.Y., HUANG Y.L., CHEN X.G., WANG C.Q. HE L.Y. Shear properties of grout-rock interface for treatment of mud inrush. *Polish Journal of Environmental Studies*, **31** (2), 1783, **2022**.
 8. WANG Y.C., YIN X., GENG F., JING H.W., SU H.J., LIU R.C. Risk assessment of water inrush in karst tunnels based on the efficacy coefficient method. *Polish Journal of Environmental Studies*, **26** (4), 1765, **2017**.
 9. WU J., ZHOU Z.F., ZHUANG C. A combined analytical-numerical method for groundwater inflow into circular tunnels in drained conditions. *Hydrogeology Journal*, **29** (7), 2529, **2021**.
 10. WAN X., DING J.W., JIAO N., SUN S., LIU J.Y., GUO Q.Y. Observed performance of long-zoned excavation with suspended waterproof curtain in Yangtze River floodplain. *Journal of Performance of Constructed Facilities*, **36** (3), 04022018, **2022**.
 11. GOODMAN R.E., MOYE D.G., SCHALKWYK A.V., JAVANDEL I. Groundwater inflow during tunnel driving. *Engineering Geology*, **2** (1), 39, **1965**.
 12. LEI S.Z. An analytical solution for steady flow into a tunnel. *Ground Water*, **37** (1), 23, **1999**.
 13. KOLYMBAS D., WAGNER P. Groundwater ingress to tunnels - The exact analytical solution. *Tunnel and Underground Space Technology*, **22** (1), 23, **2007**.
 14. LI P.F., WANG F., LONG Y.Y., ZHAO X. Investigation of steady water inflow into a subsea grouted tunnel. *Tunnel and Underground Space Technology*, **80**, 92, **2018**.
 15. ZHOU J.Q., LIU H.B., LI C.D., HE X.L., TANG H.M., ZHAO X.J. A semi-empirical model for water inflow into a tunnel in fractured-rock aquifers considering non-Darcian flow. *Journal of Hydrology*, **597**, 126149, **2021**.
 16. LI L.P., YANG G.Y., LIU H.L., SONG S.G., FAN H.Y. A quantitative model for the geological strength index based on attribute mathematics and its application. *Bulletin of Engineering Geology and the Environment*, **80** (9), 6897, **2021**.
 17. WU J., ZHOU Z.F., ZHUANG C. A combined analytical-numerical method for groundwater inflow into circular tunnels in drained conditions. *Hydrogeology Journal*, **29** (7), 2529-2543, **2021**.
 18. TU W.F., LI L.P., ZHOU Z.Q., SHANG C.S. Thickness calculation of accumulative damaged zone by rock mass blasting based on Hoek-Brown failure criterion. *International Journal of Geomechanics*, **22** (2), 04021273, **2022**.
 19. XU Z.H., BU Z.H., GAO B., PAN D.D., LIN P., NIE L.C. Sensitivity analysis and prediction method for water inflow of underground oil storage caverns in fractured porous media. *International Journal of Geomechanics*, **21** (2), 04020251, **2021**.
 20. CHENG P., ZHAO L.H., Li Q., LI L., ZHANG S.Y. Water inflow prediction and grouting design for tunnel considering nonlinear hydraulic conductivity. *KSCE Journal of Civil Engineering*, **23** (9), 4132, **2019**.
 21. COOLEY T. Engineering approaches to conditions created by a combination of karst and faulting at a hospital in Birmingham, Alabama. *Engineering Geology*, **65** (2), 197, **2002**.
 22. WU Y.S. Numerical simulation of single-phase and multiphase non-Darcy flow in porous and fractured reservoirs. *Transport in Porous Media*, **49** (2), 209, **2002**.
 23. WANG Y., QIN F., XIA Z.H., NI X.D. Non-Darcy flow model and numerical simulation for prediction water inflow in deep tunnel. *Chinese Journal of Rock Mechanics and Engineering*, **31** (9), 1862, **2012**.
 24. SHI W.H., YANG T.H., LIU H.L., YANG B. Numerical modeling of non-Darcy flow behavior of groundwater outburst through fault using the Forchheimer equation. *Journal of Hydrology Engineering*, **23** (2), 04017062, **2018**.
 25. YANG G.Y., CHE C.H., LIU S.C. Numerical simulation of forecasting water inrush volume from fault. *Journal of Mining and Safety Engineering*, **27** (3), 351, **2010**.
 26. JIANG X.W., WANG X.S., WAN L. Semi-empirical equations for the systematic decrease in permeability with depth in porous and fractured media. *Hydrogeology Journal*, **18** (4), 839, **2010**.
 27. AMELI A.A., MCDONNELL J.J., BISHOP K. The exponential decline in saturated hydraulic conductivity with depth: a novel method for exploring its effect on water flow paths and transit time distribution. *Hydrological Processes*, **30** (14), 2438, **2016**.
 28. RUMYNIN V.G., LESKOVA P.G., SINDALOVSKIY L.N., NIKULENKOV A.M. Effect of depth-dependent hydraulic conductivity and anisotropy on transit time distributions. *Journal of Hydrology*, **579**, 124161, **2019**.